Numerical computation of the spatial decaying wave characteristics for the design of locally resonant acoustic metamaterials

IOP Conf. Series: Journal of Physics: Conf. Series **1264** (2019) 012015 doi:10.1088/1742-6596/1264/1/012015

Numerical computation of the spatial decaying wave characteristics for the design of locally resonant acoustic metamaterials

M Miksch, J D Perez Ramirez, G Müller

Chair of Structural Mechanics, Technical University Munich, Arcisstrasse 21, 80333 München, Germany

E-mail: matthias.miksch@tum.de

Abstract. In structural dynamics, periodic resonant inclusions are widely used to improve the vibro-acoustic properties of lightweight structures. Depending on the design of these inclusions, the wave propagation in the structure is modified for specific frequency ranges and stop bands, where in theory no free wave propagation is possible, can be generated. The Wave Finite Element Method (WFEM) investigates the wave propagation in periodic structures based on a Finite Element (FE) model of a single unit cell. Using the direct approach of the WFEM, it is possible to depict the wave characteristics in the frequency range of the resonant frequency of the inclusions. Consequently, a spatial decay for the different wave types can be determined in the frequency range of the potential stop band. The frequency dependent decay characteristics can be used to evaluate the performance of the resonant inclusions and find optimal parameters for the desired application of the metamaterial. The procedure is applied to design beam-like resonators and find an optimal resonator spacing for a beam-like acoustic metamaterial. For a fixed percentage of added mass, the spacing of the resonators can be adjusted to optimize the maximum spatial decay or the stop band size.

1. Introduction

Locally resonant materials show a high potential for tuning the vibro-acoustic properties of structures in specific frequency ranges. Due to periodicity, Bragg scattering and negative interference can suppress free wave propagation in certain frequency ranges. While these interference effects depend on the length scale of the periodicity, resonant inclusions can generate stop bands independent of the length scale of the periodicity [1]. Furthermore, locally resonant behavior can improve vibro-acoustic properties of structures beyond the limits of conventional materials [2]. Accordingly, locally resonant materials show high potential for improving vibro-acoustic properties of lightweight structures [3–12].

There are different methods to compute the wave propagation in periodic structures. For simple periodic structures, there exist analytical solutions [1, 13, 14]. For more complex periodic structures, transfer matrix approaches, where the left and right states are related by the Floquet theorem [15], are widely used [16]. [17] used such an approach to compute the wave propagation in periodic beam-like structures. Another possibility is the receptance method introduced by [18]. [19] combined the ideas of [18] with the use of finite elements (FE) to compute the propagation constants in skin-rib structures.

Combining the transfer matrix approach with conventional FE formulations has been established as the wave finite element method (WFEM) [22] and has been used in many applications for computing the wave propagation in periodic structures. The great advantage is that only a FE-model of single unit cell of the periodic structure is modeled and that standard element libraries for finite element formulations can be used. Compared to other approaches this yields an easy use and a wide range of applications. [20] computes the wave propagation in beam systems with periodic supports. [21] applied the methodology to simulate vibrations in railway tracks. There also exist studies about two dimensional laminated plates [22–24] and honeycomb structures [25]. [4–7] use the WFEM to compute the phase and attenuation characteristics for beams with periodically attached tuned mass dampers (TMD) and [4] shows the influence of different damping ratios on the phase and attenuation. It can be shown that TMDs generate stop bands for longitudinal [5] and bending waves [6] in the vicinity of the resonance frequency of the TMD.

There are two different approaches to solve the eigenvalue problem describing the wave propagation [18]. First, the inverse approach where frequencies of free wave propagation are computed by assuming purely imaginary propagation constants. Second, the direct approach, where for every frequency of interest a complex propagation constant is computed and therefore, besides the phase information, also decaying properties at different frequencies can be estimated. The inverse approach can be used to compute the wave solutions of the undamped waves and is therefore commonly used to show in which frequency ranges free wave propagation is possible [3, 8–12]. In contrast, the direct approach computes all wave solutions and thus also determines the decaying wave solutions. The direct approach is usually used for computing the forced response of periodic structures, where also the wave solutions with decaying characteristics are necessary. The direct approach can be reformulated to overcome ill-conditioning by exploiting the symplectic property of the underlying eigenvalue problem [27]. [28] shows a condensed WFEM which reduces the modal space and therefore reduces the computational effort.

The benefit of the direct approach is that damping characteristics in the frequency range of potential stop bands can be determined. In this contribution, we investigate the influence of local resonators on the wave solutions of an Euler-Bernoulli beam using the direct approach. At first, the theoretical background of the WFEM is summarized to show how the phase and spatial decaying characteristics can be extracted from the wave solutions. Second, the influence of local resonances on the wave solutions of an Euler-Bernoulli beam is shown using the WFEM. In a next step, the wave solutions of discrete TMDs and beam-like resonators are compared. The wave characteristics are evaluated in the vicinity of the resonance frequency of the local resonator to show how the modeling of the TMD influences the stop band characteristics. In the end, the benefit of the spatial decay characteristic for the design optimization of beam like resonators is highlighted and an optimal TMD spacing for beam-like resonators is derived based on the spatial decaying characteristics.

2. The Wave Finite Element Method (WFEM)

Due to the periodicity of the structure, it is sufficient to consider a small segment of finite length (unit cell) to compute the harmonic wave propagation in the overall structure. Based on the Floquet theorem [15], the solution of the state variables in a periodic structure is periodic itself and only varies by an exponential term with respect to the length of the unit cell.

$$u(x+L) = u(x)\, e^{-i\kappa L} = u(x)\, \mu \tag{1}$$

κ is the wavenumber and L is the length of the unit cell. [29] derived a similar relation for the motion of electrons in three-dimensional lattices. According to the derivation of [15] and [29], (1) is sometimes called Floquet theorem for one-dimensional periodicity and Bloch theorem for

higher dimensional periodicity. Applying (1), the state vectors of two neighboring unit cells can be related (see figure 1).

$$\begin{bmatrix}\mathbf{q_L}\\ \mathbf{F_L}\end{bmatrix}_{N+1} = \begin{bmatrix}\mathbf{q_R}\\ -\mathbf{F_R}\end{bmatrix}_{N} = \mu \begin{bmatrix}\mathbf{q_L}\\ \mathbf{F_L}\end{bmatrix}_{N} \tag{2}$$

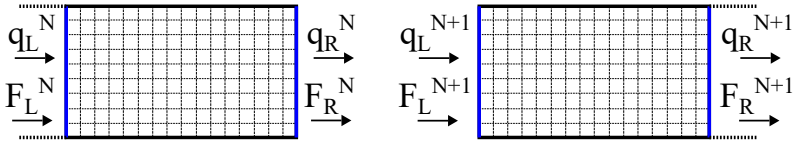

Figure 1. Deformations $\mathbf{q}$ and forces $\mathbf{F}$ of two neighboring unit cells; subscripts correspond to the location in a unit cell (left, interior or right) and the superscripts identify the unit cell.

Using a finite element model of the unit cell, the equation for time harmonic wave propagation can be set:

$$\underbrace{(-\omega^2\mathbf{M} \pm i\omega\mathbf{C} + \mathbf{K})}_{\mathbf{S}(\omega)}\mathbf{q} = \mathbf{F}\ . \tag{3}$$

$\mathbf{M}$, $\mathbf{C}$ and $\mathbf{K}$ describe mass, damping and stiffness matrices, respectively. The resulting dynamic stiffness matrix $\mathbf{S}$ can be sorted with respect to the left ($\mathbf{q_L}$), internal ($\mathbf{q_I}$) and right ($\mathbf{q_R}$) degrees of freedom.

$$\begin{bmatrix}\mathbf{S_{LL}} & \mathbf{S_{LR}} & \mathbf{S_{LI}}\\ \mathbf{S_{RL}} & \mathbf{S_{RR}} & \mathbf{S_{RI}}\\ \mathbf{S_{IL}} & \mathbf{S_{IR}} & \mathbf{S_{II}}\end{bmatrix}\begin{bmatrix}\mathbf{q_L}\\ \mathbf{q_R}\\ \mathbf{q_I}\end{bmatrix} = \begin{bmatrix}\mathbf{F_L}\\ \mathbf{F_R}\\ \mathbf{0}\end{bmatrix}\ . \tag{4}$$

As described in [22], the interior degrees of freedom can be condensed as $\mathbf{q_I} = -\mathbf{S_{II}}^{-1}(\mathbf{S_{IL}}\mathbf{q_L} + \mathbf{S_{IR}}\mathbf{q_R})$. This results in the reduced system of equations.

$$\begin{bmatrix}\tilde{\mathbf{S}}_{\mathbf{LL}} & \tilde{\mathbf{S}}_{\mathbf{LR}}\\ \tilde{\mathbf{S}}_{\mathbf{RL}} & \tilde{\mathbf{S}}_{\mathbf{RR}}\end{bmatrix}\begin{bmatrix}\mathbf{q_L}\\ \mathbf{q_R}\end{bmatrix} = \begin{bmatrix}\mathbf{F_L}\\ \mathbf{F_R}\end{bmatrix} \quad \text{with} \quad \tilde{\mathbf{S}}_{\mathbf{ij}} = \mathbf{S_{ij}} - \mathbf{S_{iI}}\mathbf{S_{II}}^{-1}\mathbf{S_{Ij}} \tag{5}$$

Reordering leads on to the relation of the state variables of two neighboring cells based on the FE model of the unit cell. This relation is described by the transfer matrix $\mathbf{T}$.

$$\begin{bmatrix}\mathbf{q_L}\\ \mathbf{F_L}\end{bmatrix}_{N+1} = \begin{bmatrix}-\tilde{\mathbf{S}}_{\mathbf{LR}}^{-1}\tilde{\mathbf{S}}_{\mathbf{LL}} & \tilde{\mathbf{S}}_{\mathbf{LR}}^{-1}\\ -\tilde{\mathbf{S}}_{\mathbf{RL}} + \tilde{\mathbf{S}}_{\mathbf{RR}}\tilde{\mathbf{S}}_{\mathbf{LR}}^{-1}\tilde{\mathbf{S}}_{\mathbf{LL}} & -\tilde{\mathbf{S}}_{\mathbf{RR}}\tilde{\mathbf{S}}_{\mathbf{LR}}^{-1}\end{bmatrix}\begin{bmatrix}\mathbf{q_L}\\ \mathbf{F_L}\end{bmatrix}_{N} = \mathbf{T}(\omega)\begin{bmatrix}\mathbf{q_L}\\ \mathbf{F_L}\end{bmatrix}_{N} \tag{6}$$

Combining the Floquet theorem (2) and (6) yields an eigenvalue problem that describes the wave solutions of the infinite structure.

$$\mu\begin{bmatrix}\mathbf{q_L}\\ \mathbf{F_L}\end{bmatrix}_{N} = \mathbf{T}(\omega)\begin{bmatrix}\mathbf{q_L}\\ \mathbf{F_L}\end{bmatrix}_{N} \tag{7}$$

This transfer matrix approach which describes the relation between displacements and forces of two neighboring elements yields an ill conditioned eigenvalue problem because of the appearance of eigenvalues corresponding to displacements and forces [30]. Numerical errors in the finite element discretization might be amplified and distort the solution. To overcome this problem, different reformulations of the eigenvalue problem exist [22, 27].

The eigenvalues μ represent the different wave solutions of the structure and appear as complex conjugate pairs.

$$\mu = e^{-i\overbrace{(\kappa_R + i\kappa_I)}^{\kappa}L} = e^{-i\kappa_R L + \kappa_I L} \tag{8}$$

The exponent of the eigenvalue defines the wave type of the corresponding eigenvalue. Figure 2 illustrates the relation between the wavenumber κ and the wave types. The relative phase change of the wave solution from a unit cell to another can be retrieved from the imaginary part of the exponent of eigenvalues μ.

$$\kappa_R L = \tan^{-1}\left(\frac{\Im(\mu)}{\Re(\mu)}\right) \tag{9}$$

Respectively, the decay characteristics of the wave solutions are linked to the real part of the exponent.

$$\kappa_I L = \log(|\mu|) \tag{10}$$

To compare different configurations, the decaying characteristic is normalized with respect to the length of the unit cell to get a spatial decaying characteristic per unit length.

$$\kappa_I = \frac{\log(|\mu|)}{L} \tag{11}$$

$\lvert\mu\rvert$	κ_R	κ_I	wave type
1	$\neq 0$	0	undamped wave
$\neq 1$	$\neq 0$	$\neq 0$	damped wave
$\neq 1$	0	$\neq 0$	evanescent wave

a)

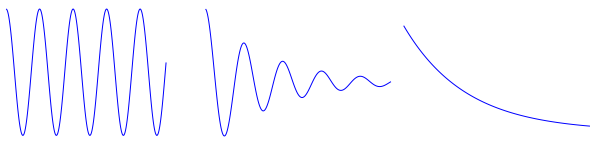

b)

Figure 2. Relation between eigenvalue μ, wavenumber κ and the different wave types of acoustic waves (a); wave forms of undamped, damped and evanescent wave (b).

3. Wave solutions of Euler-Bernoulli beam with discrete resonators

In the following, the wave solutions of an Euler-Bernoulli beam are computed with the method described in the previous section. As shown in figure 3, the beam has two degrees of freedom at each node (vertical deflection and rotation). The material parameters Young's Modulus E, density ρ and Poisson's ratio ν are also listed. The beam has a length L of 10 cm and a quadratic cross section A of 1 cm^2.

For an undamped Euler-Bernoulli beam there are four fundamental wave solutions for each frequency: two evanescent waves and two undamped waves [31]. Figure 4 shows the eigenvalues of (7) computed from $-100\ Hz$ to $100\ Hz$ in frequency steps of $0.1\ Hz$. The dashed line marks the unit circle which indicates possible locations of eigenvalues representing undamped waves. Eigenvalues located inside the unit circle represent waves traveling in the positive direction, whereas eigenvalues located outside the unit circle represent waves traveling in the negative direction. Eigenvalues located on the unit circle can represent a wave traveling in positive or negative direction. The eigenvalues representing the evanescent waves are located on the real axis. Furthermore, one can see that the wave solution for positive and negative frequencies are

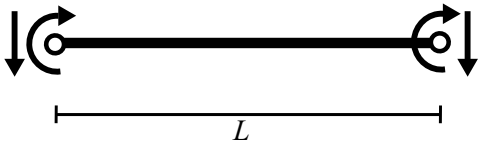

E	210 GPa
ρ	7800 kg/m^3
ν	0.3
L	10 cm
A	1 cm^2

Figure 3. Model of an Euler-Bernoulli beam with vertical and rotational degrees of freedom at each node with corresponding material and geometric properties.

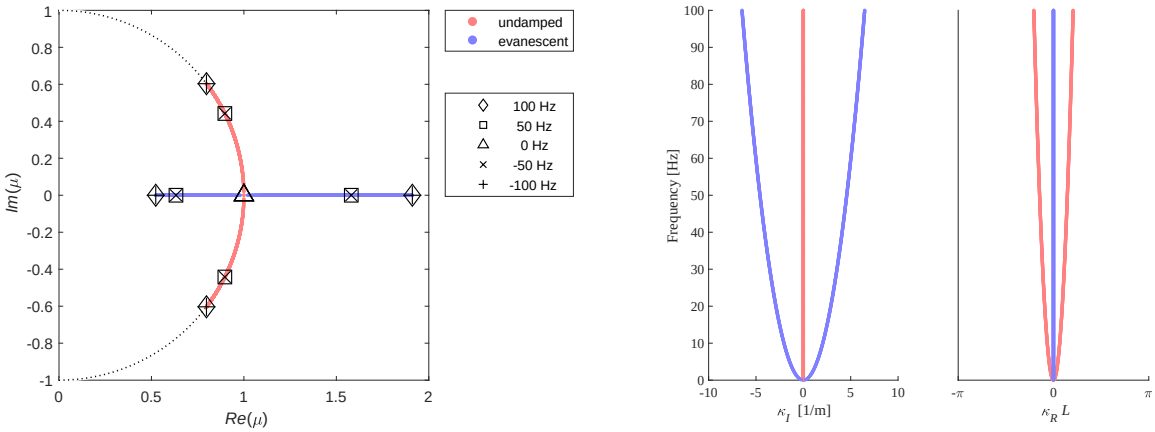

Figure 4. Solution of the eigenvalue problem (7) for the Euler-Bernoulli beam displayed in figure 3, the dashed line indicates the unit circle and the derived decay (κ_I) and phase ($\kappa_R L$) information.

the same. Figure 4 also illustrates the decay and phase information that can be extracted from the eigenvalues μ. These plots are preferably used to show the information about the frequency dependency of the wave solutions.

The Euler-Bernoulli beam is now modified by a tuned mass damper (TMD) (see figure 5). The properties of the beam are the same as in the previous model and also the wave solutions are computed for the same frequencies.

$m_{add} = m/m_{beam}$	5 %
$f_{TMD} = \frac{1}{2\pi}\sqrt{k/m}$	50 Hz
$D_{TMD} = c/(2\sqrt{km})$	1 %

Figure 5. Euler-Bernoulli beam with attached TMD and corresponding properties of the TMD; properties of the beam are the same as described in figure 3.

The mass m of the TMD is adjusted such that the mass of the overall structure is increased by 5 %. Furthermore, the resonance frequency of the TMD f_{TMD} is set to 50 Hz. Finally, the damping constant c is determined such that the critical damping ratio D_{TMD} amounts 1 %. If damping is introduced into the model, in general undamped waves do not exist. To distinguish strongly damped waves from nearly undamped waves, undamped waves are defined as having a spatial decay of less than 1% per meter.

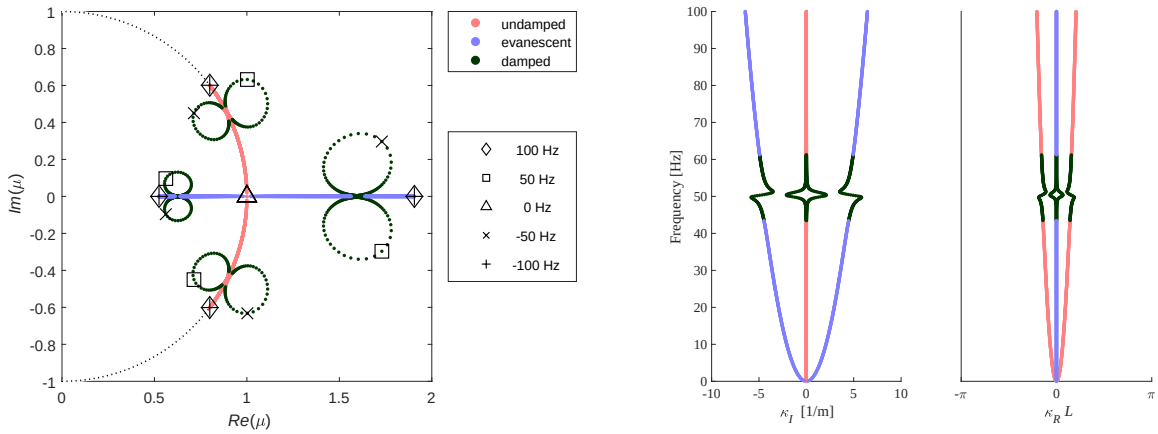

Figure 6. Eigenvalues describing the wave solutions of an Euler-Bernoulli beam with an attached TMD and corresponding spatial decay and phase information.

In Figure 6, one can see the influence of the TMD on the four wave solutions of the beam. In the frequency range around the resonance of the TMD only damped waves occur. The frequency range where no undamped waves appear is identified as stop band. Stop bands can be extracted from the decay characteristics and from the phase characteristics of the wave solutions.

One can see that the maximum spatial decaying characteristic (5.82 1/m) appears at a frequency slightly below the resonance frequency (49.7 Hz). This frequency is also the frequency where according to [32] the maximum absorption occurs. Additionally, the damped wave solutions that evolve from the originally undamped wave solutions only experience a maximum attenuation of 2.10 $1/m$ at a frequency slightly higher than the TMD resonance. Furthermore, the frequency range where the originally evanescent waves are influenced by the TMD is larger than the frequency range where the undamped waves are suppressed.

In addition, it can be concluded that if damping is present ($\mathbf{C} \neq 0$), the eigenvalue problem has also to be solved for negative frequencies ω to get all wave solutions.

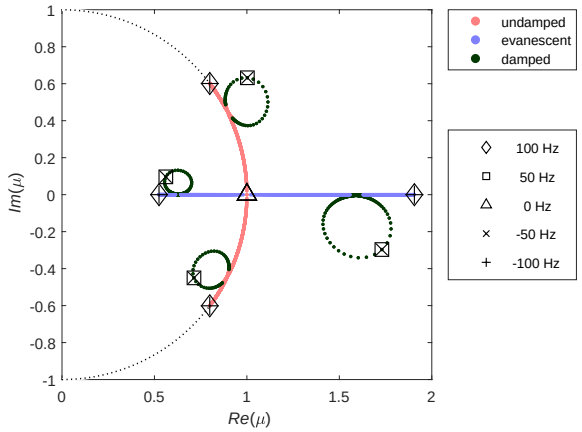

Figure 7. Eigenvalues describing the wave solutions of an Euler-Bernoulli beam with an attached TMD with complex spring stiffness $\hat{k} = k(1 + i0.02)$.

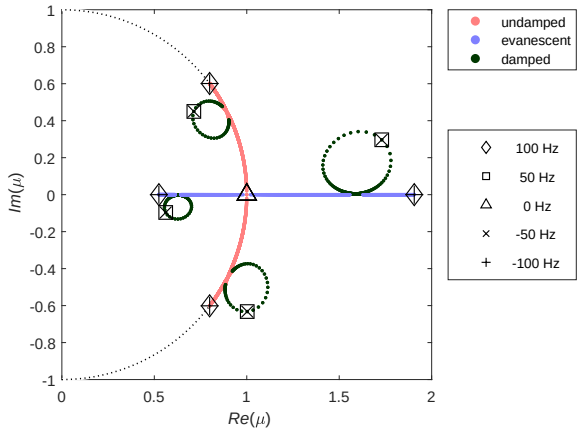

Figure 8. Eigenvalues describing the wave solutions of an Euler-Bernoulli beam with an attached TMD with complex spring stiffness $\hat{k} = k(1 - i0.02)$.

If energy dissipation with a frequency independent structural loss factor η is introduced via a complex spring stiffness $\hat{k}$, the computation has to be performed for positive frequencies with $\hat{k} = k(1 + i\eta)$ and negative frequencies with $\hat{k} = k(1 - i\eta)$ to get all wave solutions (compare figures 7 and 8).

In general, there exist wave pairs with similar shape traveling in opposite direction. These pairs have an opposite sign in the relative phase shift and the spatial decay. For undamped waves, these pairs correspond to the complex conjugate eigenvalues. For wave pairs that have a decaying characteristic, these pairs are not complex conjugates because the complex conjugate eigenvalues have the same sign in the decaying characteristic.

In practice, the geometry of the TMD also introduces a rotational inertia, which yields an additional decaying effect. Next, the wave solutions for a rotational TMD as described in figure 9 are computed.

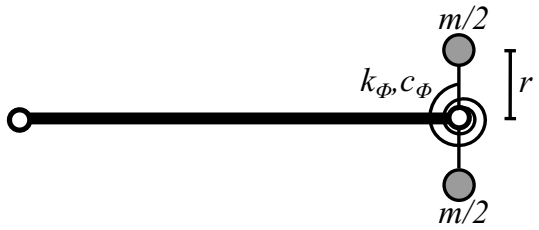

$m_{add} = m/m_{beam}$	5 %
$f_{TMD} = \frac{1}{2\pi}\sqrt{k_\Phi/(mr^2)}$	50 Hz
$D_{TMD} = c_\Phi/(2\sqrt{k_\Phi mr^2})$	1 %
r	20 cm

Figure 9. Euler-Bernoulli beam with attached rotational TMD and corresponding properties of the TMD; properties of the beam are the same as described in figure 3.

The rotational TMD has a rotational spring stiffness k_Φ as well as a damping constant c_Φ which allows to introduce a critical damping ratio D_{TMD}.

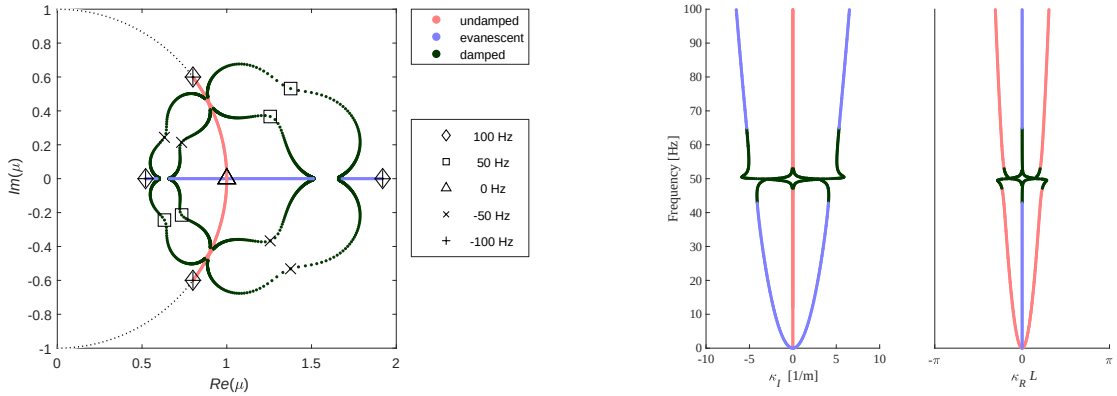

Figure 10. Eigenvalues describing the wave solutions of an Euler-Bernoulli beam with an attached rotational TMD and corresponding spatial decay and phase information.

In figure 10 the maximum spatial decay is located at 50.5 Hz, which is slightly higher than the resonance frequency of the rotational TMD. The maximum spatial decay is 5.89 $1/m$. Comparing the evolution of the damped waves solution, the rotational TMD modifies the wave solution of the Euler-Bernoulli beam differently than the vertical TMD. The wave branches in the resonance stop band have different shapes than with a vertical TMD. The rotational TMD with a large rotational inertia creates damped wave solutions that show a transitional behavior between undamped and evanescent wave solutions and vice versa.

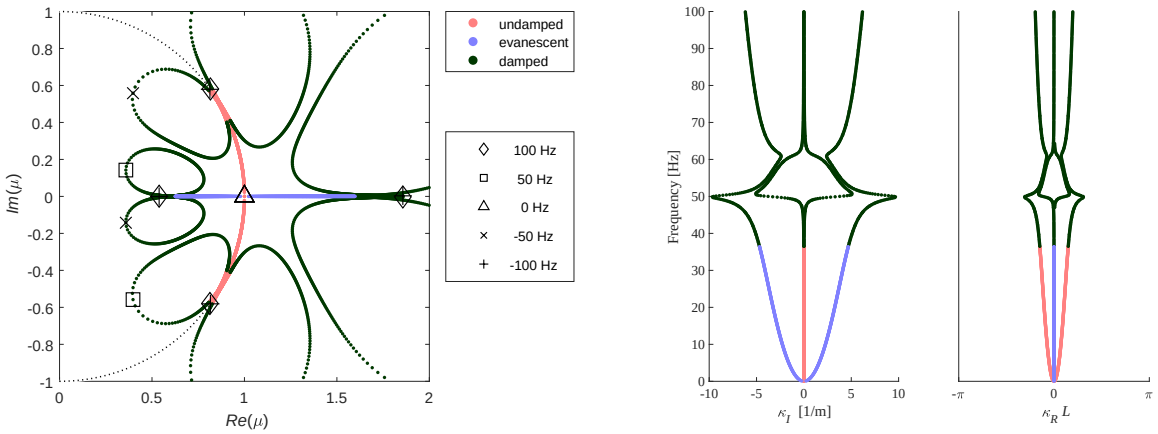

Figure 11. Eigenvalues describing the wave solutions of an Euler-Bernoulli beam with an attached vertical TMD with increased mass (50 % of the mass of the beam) and corresponding spatial decay and phase information.

The vertical TMD leaves the originally undamped and evanescent wave solutions separately, independent from the mass (see the eigenvalue plots in figures 6 and 11). The reason for this can be identified in the eigenvalue plot: the loops of damped waves, that appear in the vicinity of the resonance frequency of the TMD do not overlap. The loops marked in figure 11 are based on wave solutions of frequencies with opposite sign.

Comparing figures 6 and 11, one can see that a larger mass enhance the stop band, which was already shown by [4]. In addition, a larger mass increases the maximum spatial decay as well as the averaged spatial decay in the stop band. Furthermore, the frequency range where evanescent waves are suppressed growth more than the stop band for the undamped waves.

4. Influence of the TMD spacing on the wave solutions

In a next step, the wave solutions for beams with different lengths are computed. The total mass added by the TMD is again fixed to 5 % of the mass of the beam. Thus, the overall mass added per unit length is constant. Varying the length L is equivalent to compare different TMD spacing for a fixed percentage of additional mass.

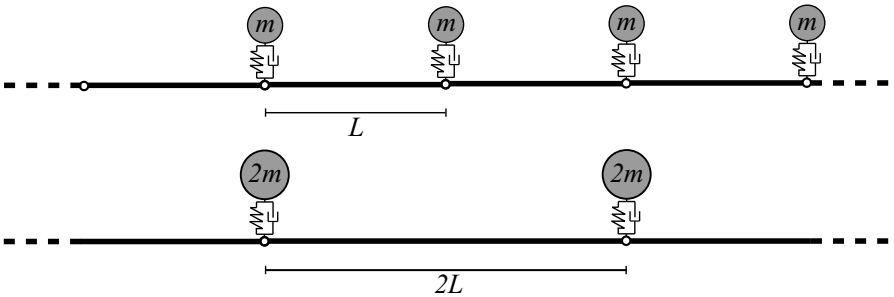

Figure 12. What is the optimal TMD spacing? Effect of doubling the beam length L (TMD spacing) on the mass of the TMD while the percentage of added mass by the TMD is fixed.

This investigation is applied to beams with a vertical and rotational TMDs as described in figures 5 and 10, respectively. Figure 13 illustrates the dependence of the stop band

characteristics on the TMD spacing L for the beam with vertical and rotational TMD for two different resonance frequencies.

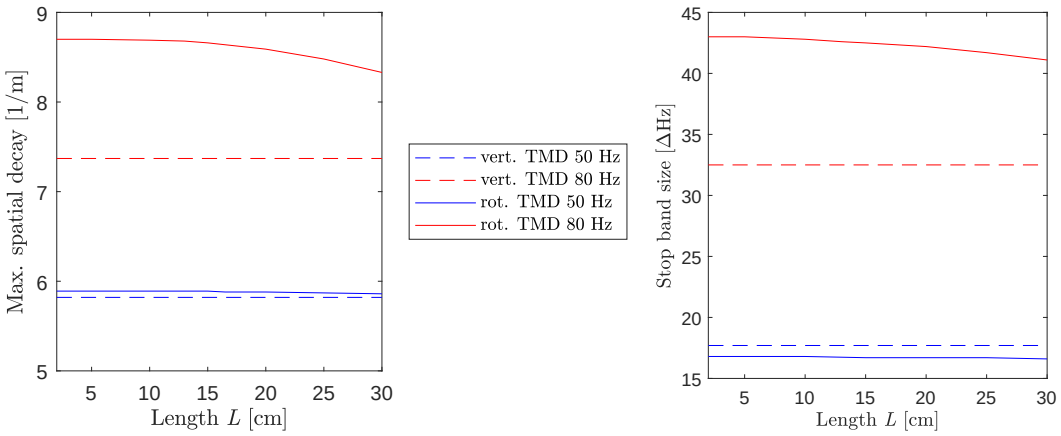

Figure 13. Influence of the TMD spacing on the stop band characteristics for a discrete vertical and rotational TMD; stop band size is defined as the frequency range where only wave solutions with a spatial decay greater than 1% exist.

The TMDs with resonance frequency of 50 Hz (marked with blue color) result in a smaller maximum decay and a smaller stop band size as the TMDs with resonance frequency of 80 Hz. Interestingly, the stop band characteristics for the vertical TMDs (dashed lines) do not vary with increasing TMD spacing. In comparison to the vertical TMD, the rotational TMD yields slightly decreasing maximum decay and stop band size when the TMD spacing increases. Therefore, using a rotational TMD the smallest possible TMD spacing maximizes the maximum spatial decay and the stop band size.

In many applications, local resonances are introduced by integrating beam-like structures into the main structure. Therefore, the discrete TMD is replaced by an Euler-Bernoulli beam as demonstrated in figure 14.

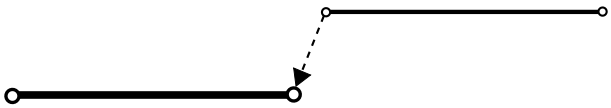

$f_{TMD-beam} = \frac{1.875^2}{2\pi L_{TMD}^2}\sqrt{\frac{EI_{TMD}}{\rho A_{TMD}}}$	50 Hz
$m_{add} = m_{TMD-beam}/m_{beam}$	5 %

Figure 14. Model of an Euler-Bernoulli beam with attached Euler-Bernoulli beam that acts as a TMD; cross section A of the main beam is 1 cm^2.

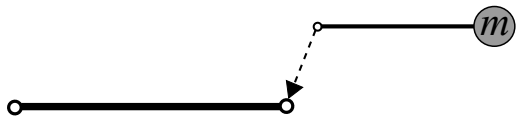

$f_{TMD} = \frac{1}{2\pi}\sqrt{\frac{3EI_{TMD}}{L_{TMD}^3(m+0.24m_{TMD-beam})}}$	50 Hz
$m_{add} = (m + m_{TMD-beam})/m_{beam}$	5 %

Figure 15. Euler-Bernoulli beam with attached TMD-beam with additional end mass and corresponding properties of the TMD-beam.

The material and geometric properties of the main beam are the same as previously described in figure 3, except that the damping is included by a complex Young's Modulus $\hat{E} = E(1 + i\eta)$,

where η is the structural loss factor and has a fixed value of 0.001. The smaller beam that acts as a local resonator consists of the same material as the main beam. Knowing the desired (first) eigenfrequency and the mass of the TMD-beam, the necessary length and the cross section of the TMD-beam can be computed. To derive the dependence between the geometry and the resonance frequency, we assume that the TMD-beam behaves as a clamped-free Euler-Bernoulli beam [35]. The resulting TMD-beam can be comparably long with respect to the length of the unit cell. This might be infeasible for practical applications. Therefore, a part of the additional mass should be added as concentrated mass to the end of the TMD-beam (see figure 15).

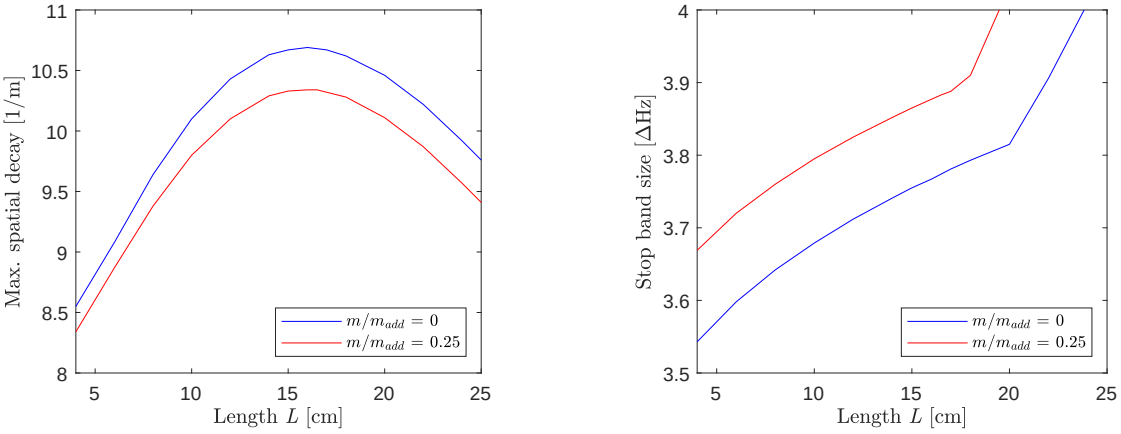

Figure 16. Comparison of the stop band characteristics of an Euler-Bernoulli beam with attached TMD-beam without end mass and with end mass equal to a quarter of the total added mass; stop band size is defined as the frequency range where only wave solutions with a spatial decay greater than 1% exist.

Figure 16 compares the maximum decay in the stop band and the stop band size for a TMD-beam with and without end mass for different TMD spacings. For a better resolution in the stop band, the frequency steps are decreased from 0.1 Hz to 0.001 Hz in the frequency range from ± 48 to ± 53 Hz. The optimal spatial decay for both models occurs with a TMD spacing around a quarter of the wave length of the bending wave at resonance frequency of the TMD (16.5 cm). For smaller or larger TMD spacings the maximum spatial decay decreases. The TMD-beam without end mass shows a larger decay for all TMD spacings. With increasing TMD spacing the stop band size increases. The configuration with an additional end mass yields a larger stop band size.

Comparing the stop band characteristics of the TMD-beams to the discrete vertical or rotational TMDs with mass equal to the corresponding modal mass of the TMD beam, it seems that the stop band size is overestimated and the spatial decay underestimated by the discrete TMDs. These differences occur even if the mass of the discrete TMD is adjusted to the modal mass of the beam-like TMD (the modal mass of the first resonance of the TMD-beam without end mass is equal to the mass of the TMD-beam [34]). Furthermore, the optimal TMD spacing for the beam-like resonators differs from the optimal TMD spacing for discrete TMDs.

In the following, the influence of a varying end mass on the stop band characteristics is investigated. The stop band characteristics are computed for different ratios of end mass to total added mass (m/m_{add}). As previously, the amount of total added mass by the TMD-beam is fixed to 5 % of the mass of the main beam.

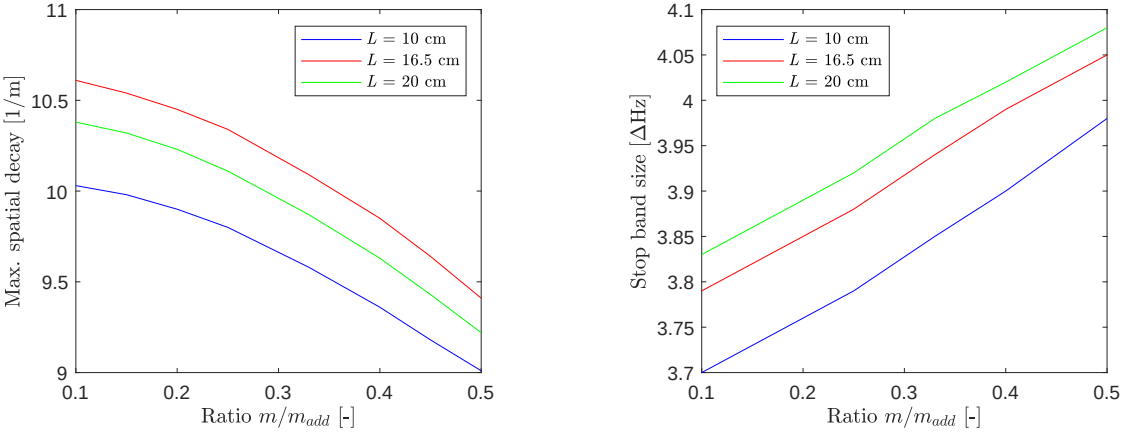

Figure 17. Comparison of the stop band characteristics of Euler-Bernoulli beams of different length with attached TMD-beams with different ratio of end mass to total added mass; stop band size is defined as the frequency range where only wave solutions with a spatial decay greater than 1% exist.

Figure 17 illustrates the maximum decay and the stop band size. The maximum decay in the stop band decreases with increasing end mass for TMD spacings of 10, 16.5 and 20 cm. As previously observed, the optimal TMD spacing for a maximum decay is 16.5 cm, which is a quarter of the wavelength of the bending wave at 50 Hz. For each TMD spacing, the stop band size increases with increasing end mass.

Concluding from these examples, for a maximum spatial decay at the resonance frequency of the beam-like resonator, the beam-like resonator should not have a concentrated end mass. However, for a maximum stop band size most of the additional mass should be placed as concentrated mass at the end of the beam.

5. Conclusions

We showed how the WFEM can be used to extract the spatial decay characteristics of periodic structures. Besides the location of the stop band, the spatial decay characteristics also provide information about the wave solutions that exist in the frequency range of stop bands. The spatial decay reproduces well known characteristic properties of resonant materials, e.g. the frequency of maximum absorption. Based on the spatial decay, the influence of discrete vertical and rotational TMDs on the wave solution of an Euler-Bernoulli beam has been shown. Furthermore, the comparison of the discrete TMD with a beam-like TMD showed that there are significant differences in the stop band characteristics, even if the mass of the discrete TMD is adjusted to the modal mass of the beam-like TMD. This fact needs to be considered in order to increase the compliance of the wave solutions of a real TMD design and a simplified computational model.

In addition, an optimal TMD spacing can be derived based on the spatial decay of the wave solutions. The optimal TMD spacing for a maximum decay at the resonance of the TMD is one quarter of the bending wavelength at the resonance frequency of the resonator. Beam-like resonators with an additional end mass introduce a smaller maximum decay but increase the stop band size (assuming the total amount of added mass remains unchanged). Concluding, the spatial decay seems to be a very useful quantity to compare different designs and it might be used as objective function to optimize the frequency dependent performance of acoustic metamaterials in the frequency range of potential stop bands.

Further investigation will be performed to identify to what extent the design rules derived from the characteristics of the wave solutions of infinite structures are also valid for realistic finite structures.

Acknowledgments
This project is funded by the Bavarian Ministry of Economics within the scope of the Ludwig-Bölkow-Campus (LBC) in Ottobrunn/Taufkirchen (Förderkennzeichen: LABAY92C).

References

[1] Brillouin L 1946 *Wave propagation in periodic structures* (New York: McGraw-Hill)
[2] Liu Z, Zhamg X, Mao Y, Zhu Y Y, Yang Z, Chan C T and Sheng P 2000 *Science* **289**(5485) 1734-6
[3] Claeys C C, Sas P and Desmet W 2011 *On the potential of local resonators to obtain low-frequency band gaps in periodic lightweight structures* Proc. ECCOMAS, Corfu
[4] Claeys C C, Vergote K, Sas P and Desmet W 2013 *J. Sound Vibr.* **332** 1418-36
[5] Xiao Y, Wen J and Wen X 2012 *New J. Physics* **14** 033042
[6] Xiao Y, Wen J and Wen X 2012 *Physics L. A* **376**(16) 1384-90
[7] Xiao Y, Wen J, Yu D and Wen X 2013 *J. Sound Vibr.* **332** 867-93
[8] Claeys C C, Sas P and Desmet W 2014 *J. Sound Vibr.* **333**(14) 3203-13
[9] Claeys C C, Deckers E, Pluymers B and Desmet W 2016 *Mech. Sys. Sign. Process.* **70-71** 853-80
[10] Claeys C C, Deckers E, Pluymers B and Desmet W 2016 *ATZ Extra* bf 1(1) 50-3
[11] Melo N F, Claeys C C, Deckers E, Pluymers B and Desmet W 2016 *SAE Int. J. Pass. Cars - Mech. Sys.* **9**(3) 1013-19
[12] Claeys C C, Rocha de Melo Filho N G, Van Belle L, Deckers E and Desmet W 2017 *Ext. Mech. L.* **12** 7-22
[13] Graff K F 1975 *Wave Motion in Elastic solids* (New York: Dover Publications)
[14] Cremer L, Heckl M and Petersson B A T 2005 *Structure-Borne Sound*, $3^r d$ ed. (Berlin: Springer)
[15] Floquet G 1883 *Ann. scientifiques de l'É.N.S* 2^e *série* **12** 47-88
[16] Thompson W T 1950 *Journal of Applied Physic* **21** 89-93
[17] Lin Y K and McDaniel T J 1969 *Journal of Engineering for Industry* **91** 1133-41
[18] Mead D J 1973 *J. Sound Vibr.* **27**(2) 235-60
[19] Orris R M and Petyt M 1974 *J. Sound Vibr.* **33**(2) 223-36
[20] Abdel-Rahman A 1979 Matrix analysis of wave propagation in periodic systems *University of Southampton, Ph.D. thesis*
[21] Thompson D J 1993 *J. Sound Vibr.* **161** 421-46
[22] Mace B R, Duhamel D, Brennan M J and Hinke L 2005 *J. Acoust. Soc. Am.* **170** 2835-43
[23] Mace B R and Manconi E 2008 *J. Sound Vibr.* **318** 884-902
[24] Manconi E, Mace B R and Garziera R 2013 *J. Sound Vibr.* **332**(7) 1704-11
[25] Ruzzene M, Scarpa F and Soranna F 2003 *Smart Mat. Struct.* **12** 363– 372
[26] Mead D J 1996 *J. Sound Vibr.* **190**(3) 495-524
[27] Zhong W X and Williams F W 1995 *J. Sound Vibr.* **181**(3) 485-501
[28] Zhou C 2014 Wave and modal approach for multi-scale analysis of periodic structures *Ecole Centrale de Lyon, Ph.D. thesis*
[29] Bloch F 1929 *Zeitsch. Physik* **52** 555-600
[30] Pestel E C and Leckie F A 1963 *Matrix methods in elastomechanics* (New York: McGraw-Hill)
[31] Cremer L and Heckl M 1967 *Köperschall. Physikalische Grundlagen und Technische Anwendung* (Berlin: Springer)
[32] Den Hartog J P 1956 *Mechanical Vibrations* (New York : McGraw- Hill)
[33] Duhamel D, Mace B R and Brennan M J 2006 *J. Sound Vibr.* **294** 205-20
[34] Howard C Q 2007 *J. Sound Vibr.* **301** 410-4
[35] Blevins R D 2016 *Formulas for dynamics, acoustics and vibration* (Hoboken: Wiley)